Journal of Environmental Management 357 (2024) 120780

Contents lists available at ScienceDirect

Journal of Environmental Management

journal homepage: www.elsevier.com/locate/jenvman

Research article

Responses of streamflow to forest expansion in a typical subhumid watershed under future climate conditions

Jia Yang [a,*], Abigail Winrich [a], Tian Zhang [a], Lei Qiao [b], Chris Mattingly [c], Chris Zou [a]

[a] Department of Natural Resource Ecology and Management, Oklahoma State University, Stillwater, OK, 74078, USA
[b] Oklahoma Water Resources Center, Oklahoma State University, Stillwater, OK, 74078, USA
[c] Norman Utilities Authority, Norman, OK, 73070, USA

ARTICLE INFO

Keywords:
Eastern redcedar
The soil & water assessment tool
Land cover change
Woody plant encroachment
Afforestation
Water resources

ABSTRACT

Water availability in the subhumid region is highly vulnerable to frequent droughts. Water scarcity in this region has become a limiting factor for ecosystem health, human livelihood, and regional economic development. A notable pattern of land cover change in the subhumid region of the United States is the increasing forest area due to afforestation/reforestation and woody plant encroachment (WPE). Given the distinct hydrological processes and runoff generation between forests and grasslands, it is important to evaluate the impacts of forest expansion on water resources, especially under future climate conditions. In this study, we focused on a typical subhumid watershed in the United States – the Little River Watershed (LRW). Utilizing SWAT + simulations, we projected streamflow dynamics at the end of the 21st century in two climate scenarios (RCP45 and RCP85) and eleven forest expansion scenarios. In comparison to the period of 2000–2019, future climate change during 2080–2099 will increase streamflow in the Little River by 5.1% in the RCP45 but reduce streamflow significantly by 30.1% in the RCP85. Additionally, our simulations revealed a linear decline in streamflow with increasing forest coverage. If all grasslands in LRW were converted into forests, it would lead to an additional 41% reduction in streamflow. Of significant concern is Lake Thunderbird, the primary reservoir supplying drinking water to the Oklahoma City metropolitan area. Our simulation showed that if all grasslands were replaced by forests, Lake Thunderbird during 2080–2099 would experience an average of 8.6 years in the RCP45 and 9.4 years in the RCP85 with water inflow amount lower than that during the extreme drought event in 2011/2012. These findings hold crucial implications for the formulation of policies related to afforestation/reforestation and WPE management in subhumid regions, which is essential to ensuring the sustainability of water resources.

1. Introduction

Climate change exerts profound impacts on the water cycle, significantly affecting both natural ecosystems and human communities in the United States (Payton et al., 2023). Model projections for the end of the 21st century indicated an anticipated decrease of 12–28% in river flow within the Arkansas River Basin in the central U.S. under future climate conditions (Yang et al., 2023). Given the importance of surface water for municipal water supply and agricultural use in the central U.S., it is imperative to assess the impacts of land cover changes and land management policies on streamflow under future climate conditions. A potential type of land cover change in the central U.S. is the expansion of woody plant coverage due to juniper encroachment and forest plantation (DeSantis et al., 2011; Zou et al., 2016).

Recent estimates indicate that the Earth's land ecosystems have the capacity to support another 0.9 billion hectares of forests, which is equivalent to over 200 Gt of carbon or 25% of the carbon storage in the atmosphere (Bastin et al., 2019). Afforestation and reforestation represent critical natural climate solutions to combat climate change and mitigate climate warming (Griscom et al., 2017; Robertson et al., 2022; Xu et al., 2023). According to the FAO The State of the World 's Forests (2022); FAO, 2022), global forest area is shrinking, with 420 million ha lost through deforestation during 1990–2020. Moreover, satellite-based study revealed a reduction in global forest area from 2000 to 2012, which experienced 230 M ha forest losses and 80 M ha gains (Hansen et al., 2013). These changes in forest coverage exert a profound influence on global climate conditions through a series of biophysical and biogeochemical processes (Alkama and Cescatti, 2016; Canadell and

* Corresponding author. Department of Natural Resource Ecology and Management Oklahoma State University, 008 Ag Hall, Stillwater, OK, 74078, USA.
E-mail address: jia.yang11@okstate.edu (J. Yang).

https://doi.org/10.1016/j.jenvman.2024.120780
Received 5 November 2023; Received in revised form 14 March 2024; Accepted 27 March 2024
Available online 3 April 2024

Raupach, 2008; Cerasoli et al., 2021). Over the period of 2001–2019, global forest loss resulted in gross greenhouse gas (GHG) emissions of 8.1 Gt CO_2e yr^{-1} (Harris et al., 2021). However, amidst these challenges, global forests continued to function as a substantial and persistent carbon sink (Pan et al., 2011) and sequestrated carbon from the atmosphere at a rate of 15.6 Gt CO_2e yr^{-1} in the first two decades of this century (Harris et al., 2021).

Afforestation/reforestation efforts in the United States hold promising potential, capable of sequestrating 13–21 Tg of Carbon per year in the topsoil, accounting for 10% of the US forest carbon sink (Nave et al., 2018). According to the spatial dataset of afforestation/reforestation opportunities developed by Griscom et al. (2017), the subhumid southcentral United States, especially the eastern part of the southern Great Plains (SGP) in Oklahoma, Texas, and Kansas, have a vast area for potential afforestation/reforestation (see Atlas of Forest Landscape Opportunities, https://www.wri.org/applications/maps/flr-atlas). This region corresponds significantly with the forest-grassland transition zone in the United States (Joshi et al., 2019; Starr et al., 2019).

The forest-grassland transition zone in the subhumid United States encompasses several major metropolitan areas, such as Oklahoma City and Tulsa in Oklahoma, and Dallas-Fort Worth in Texas. Vegetation in this region is featured by a diverse mix of forests, savanna, and grasslands. Prominent tree species in this area include post oak (*Quercus stellata*), black hickory (*Carya texana*), and blackjack oak (*Q. marilandica*) (Karki and Hallgren, 2015). In the Cross Timbers ecoregion and the broader subhumid region in the United States, recurring droughts represent a significant natural disturbance (Ansley et al., 2023), imposing considerable impacts on the availability of surface water resources (Livneh and Hoerling, 2016). The duration and intensity of drought is naturally variable, but both have been escalating in response to climate change. One early example of this is the prolonged water deficit and high temperature in the 1930s, which severely diminish water availability and contributed to the notorious "Dust Bowl" event (Schubert et al., 2004). At a sub-seasonal scale, flash droughts have been becoming more frequent over recent decades (Christian et al., 2019). During the 2011/2012 Great Plains drought, the water level of Lake Thunderbird (a major drinking water source for Midwest City, Del City, and Norman in the Oklahoma City metropolitan areas) dropped to 2.1 m below the recommended conservation pool, underscoring the profound impacts of drought on water supply in this region. Furthermore, Yang et al. (2023) reported that future drought events will be more frequent and severe, leading to a substantial reduction in river flow and water resources availability. Therefore, ensuring a sustainable supply of surface water in the subhumid region is not only imperative for preserving ecological integrity but also essential for human livelihood and regional economic development.

Over the past few decades, the vegetation composition in the forest-grassland transition zone has undergone notable changes due to shifts in climate conditions and the suppression of fires (DeSantis et al., 2011). There has been a discernible trend of woody plant encroachment (WPE) into existing grasslands, as well as the replacement of deciduous forests by the evergreen species *Juniperus virginiana* (eastern redcedar, redcedar) (Briggs et al., 2005; Hoff et al., 2018). WPE in this region is occurring at a rate five to seven times faster than other ecoregions in the country (Archer et al., 2017; Barger et al., 2011; Wilcox et al., 2018). Eastern redcedar, which is a native species to eastern North America, is one of the major woody species encroaching into the native grasslands. Recent satellite observations indicate that an average of 40 km^2 Oklahoma grasslands have been transformed into woodlands each year over the past four decades (Wang et al., 2018a). Redcedar encroachment is expected to continue in the U.S. forest-grassland transition zone under future climate conditions (Yang et al., 2024).

Land conversion from grasslands to woodlands and forests has significant implications for hydrological processes by altering various aspects of the hydrological cycle, including evapotranspiration patterns (Huxman et al., 2005), soil moisture dynamics (Acharya et al., 2017; Zou et al., 2014), groundwater recharge (Acharya et al., 2018), and ultimately streamflow (Qiao et al., 2017; Zou et al., 2016). A prevailing consensus is that the increase in woody plant coverage would lead to elevated rates of evapotranspiration but reduced river discharge (Kishawi et al., 2023). It is important to note that previous studies examining the impacts of increased woody plant coverage on hydrological processes and river flow focused on the contemporary period without accounting for the future shift in dryness with climate change (e.g. Qiao et al., 2017; Zou et al., 2016). Given that planted trees or encroaching woody species require decades to reach their mature stage, it becomes imperative to comprehend the effects of the expanding forest area on hydrological processes under future climate change scenarios in the subhumid area. It is noteworthy that the magnitude of future forest coverage is subject to significant uncertainties. Therefore, studies that provide estimates of water resource variations across a wide spectrum of forest expansion scenarios become imperative for the development of afforestation and land management policies to balance the increases in forest coverage and water resources availability.

In this study, we selected a typical subhumid watershed in the forest-grassland transition zone, i.e., Little River watershed (LRW) in central Oklahoma, to investigate the changes in streamflow patterns in response to different levels of forest expansion and climate change. We utilized the SWAT+ (version: 6.5.6.64) to simulate streamflow in the LRW under two different climate change scenarios and eleven forest expansion scenarios. Aims of this study are to (1) evaluate the capacity of SWAT+ in simulating streamflow in the subhumid region and the impacts of forest expansion on the changes in river flow; (2) provide valuable scientific insights and evidence for informing federal and state governments in designing afforestation/reforestation policies in the subhumid region; and (3) aid in the development of land management strategies to curb the encroachment of woody plants and ensuring a sustainable water supply. The novelty of this study lies in two key aspects: First, it investigated the impacts of afforestation and woody plant encroachment on river flow and the inflow of water into Lake Thunderbird under future climate conditions. Secondly, it introduced a large spectrum of forest expansion gradient scenarios, providing support for land management agencies in devising tailored afforestation and management strategies suited to different levels of forest coverage in the subhumid region.

2. Methods and data

2.1. Study domain

We selected the Little River watershed in central Oklahoma (35.16 °N, 96.97 °W) as our study domain, which is a typical subhumid watershed situated in the transition zone between the forests in the eastern U.S. and the prairies in the Great Plains (Fig. 1). It encompasses a total area of 2528 km^2 in the Cross Timbers ecoregion. The Little River originates in Cleveland County and flows ~140 km southeastwardly until it joins the Canadian River. Eventually, it merges with the Arkansas River and the Mississippi River. Notably, Lake Thunderbird on the Little River serves as the major water source for Oklahoma City metropolitan areas of Midwest City, Del City, and Norman. According to the statistics derived from the National Land Cover Dataset (NLCD) (Homer et al., 2012), the major land cover types in the LRW are forest, grassland, and developed area, accounting for 48.48%, 39.16%, 8.46% of the watershed, respectively. In NLCD, developed area refers to areas characterized by a high percentage (30% or greater) of constructed material. The average elevation of the LRW is 315 m, with the highest elevations exceeding 370 m in the western part of the watershed and the lowest elevations below 250 m in the eastern part (Fig. S1).

Based on the gridMET climate data (Abatzoglou, 2013) during 2000–2019, the annual average temperature in the LRW was 16.8 °C, annual precipitation was 978 mm in depth (24.7×10^8 m^3 in volume), and annual potential evapotranspiration was 1574 mm. The Aridity Index (*AI*), defined as the ratio of average annual precipitation to

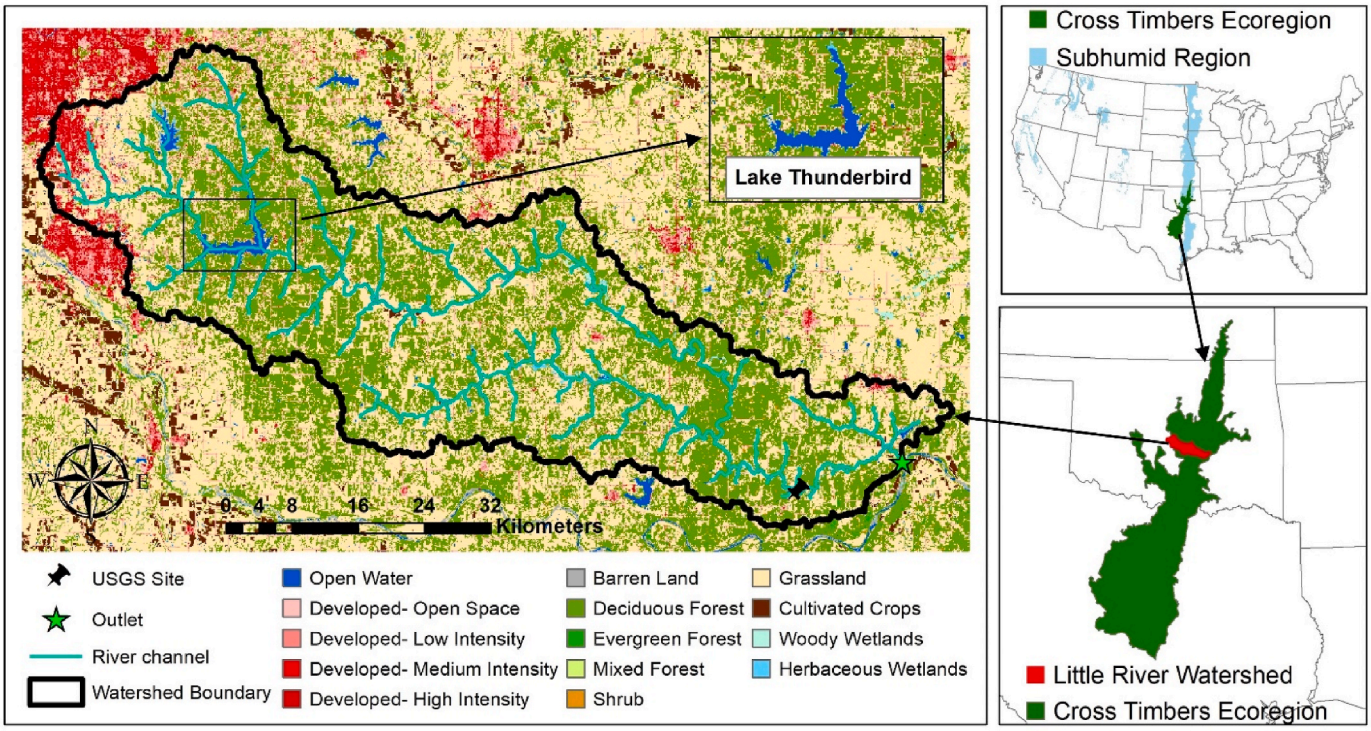

Fig. 1. Study domain of the Little River Watershed in central Oklahoma and the location of Lake Thunderbird. Land use/land cover type is from the National Land Cover Dataset (NLCD). Watershed boundary and river channels are derived from the Shuttle Radar Topography Mission (SRTM) elevation data. Distribution of the subhumid region was identified based on Aridity Index in the range between 0.5 and 0.65.

average potential evapotranspiration, was calculated to be 0.62. This value indicates that the LRW falls within the subhumid climate zone, based on the climate classification scheme proposed by Middleton and Thomas (1997). The LRW has distinct seasonal variations in temperature and precipitation (Fig. S2). The highest monthly temperatures occur in June (25.9 °C), July (28.2 °C), and August (27.8 °C), while the lowest monthly temperatures are observed in December (5.2 °C), January (4.3 °C), and February (6.2 °C). May (143 mm month^{-1} or 3.6×10^8 m^3 month^{-1}) and June (126 mm month^{-1} or 3.2×10^8 m^3 month^{-1}) receive the highest monthly precipitation, whereas November (54 mm month^{-1} or 1.4×10^8 m^3 month^{-1}), December (47 mm month^{-1} or 1.2×10^8 m^3 month^{-1}), January (36 mm month^{-1} or 0.9×10^8 m^3 month^{-1}), and February (50 mm month^{-1} or 1.3×10^8 m^3 month^{-1}) experience the lowest monthly precipitation.

2.2. Overview of the SWAT+

In this study, we employed the Soil and Water Assessment Tool + (SWAT+, version: 6.5.6.64) to conduct monthly simulations of streamflow in the LRW. SWAT is a comprehensive, semi-distributed hydrological model for simulating streamflow, nutrient, and sediment transport at the basin level across various environmental conditions and land use/management practices (Arnold et al., 2012). SWAT + represents a significant improvement over the original SWAT. The major improvement is the incorporation of the landscape units, e.g. upland areas and floodplains. This improvement enables the simulation of water and nutrient movement from the upland landscape units to the floodplains (Bieger et al., 2017). In SWAT+, the landscape units are composed of multiple Hydrologic Response Units (HRUs), which are defined as a contiguous area with similar soil, plant, topographic, and climate conditions (Bailey et al., 2020). The land areas in a subbasin are composed of landscape units. Compared to the original SWAT, the SWAT + has greater flexibility in defining aquifers, whose boundaries do not have to coincide with the boundaries of HRU, landscape units, or subbasins. The hydrologic routines in SWAT + simulate surface runoff, lateral flow, and return flow, which reach river channels and turn into streamflow.

SWAT + has been widely validated over recent years and used to simulate streamflow dynamics under climate change and forest expansion scenarios (e.g. Chawanda et al., 2020; Kiprotich et al., 2021; Pulighe et al., 2021). These studies demonstrate the robustness of SWAT + in representing the complexity of hydrological systems and providing insights into water resource management.

2.3. SWAT + input data

The key input datasets to drive SWAT + are Digital Elevation Model (DEM), land use and land cover type, soil properties, and climate conditions. The DEM data used in this study was obtained from the 30-m Shuttle Radar Topography Mission (SRTM) dataset (Rodríguez et al., 2006). The land use and land cover data was sourced from the National Land Cover Database 2019 (Homer et al. (2012)). Soil properties were derived from the gridded Soil Survey Geographic Database (gSSURGO) developed by the National Resource Conservation Service (NRCS), the United States Department of Agriculture (USDA). A soil lookup table was created to link SSURGO soil map unit key (MUKEY) to soil names in SWAT + soil table and extract soil properties. All these aforementioned datasets were converted to the same projection type of the USGS Albers Equal Area projection system. They were then resampled to a spatial resolution of 120 m to ensure data compatibility and consistency. Based on these input datasets, HRUs were delineated in SWAT+. Grids in each HRU have similar land cover type, soil type, and topographic factors (Fig. S3). Finally, a total of 5769 HRUs and 13 subbasins were generated to represent the hydrologic responses characteristics of different combinations of land use, soil properties, and topography in the LRW. We also added two reservoirs (i.e., Lake Thunderbird and Lake Stanley Draper) in the LRW, which were simply treated as impoundments without dam operations in this study.

Climate data to drive SWAT+ were collected from two sources, including the gridMET data (Abatzoglou, 2013) and the Multivariate Adaptive Constructed Analogs (MACA) v2 developed by Abatzoglou and Brown (2012), both of which have a spatial resolution of approximately 4 km. Climate variables to drive SWAT + include daily maximum/minimum temperature, precipitation, solar radiation, humidity, and wind speed. The observation-based gridMET data was used to drive SWAT + for model calibration and validation. The MACA v2 data, on the other hand, provides the downscaled climate data from Earth System Models (ESMs) under two Representative Concentration Pathways (RCP) of the CMIP5 project, i.e., RCP45 and RCP85 (Taylor et al., 2012). The MACA v2 data corrected biases in all these climate variables of the ESM simulations based on the gridMET climate conditions from 1979 to 2012. To account for the divergences in climate conditions simulated by ESMs, climate data from five ESMs were used to drive SWAT+, including bcc-CSM1 (bcc), GFDL-ESM2G (GFDL), HadGEM2-ES365 (HadGEM), IPSL-CM5A-LR (IPSL), and MIROC5 (MIROC). In the MACA v2 dataset, these five ESMs provided all necessary climate variables to drive the SWAT+. Fig. S4 shows that, during the period of 2000–2019, monthly variations of the bias-corrected climate variables from MACA v2 match the data extracted from gridMet.

In the simulation period of 2000–2019, the average CO_2 concentration was set to 390 ppm based on global CO_2 data provided by NOAA Global Monitoring Laboratory. For the simulation period of 2080–2099, CO_2 concentration was set to 535 ppm for the RCP45 and 837 ppm for the RCP85 based on the RCP database version 2.0 (https://tntcat.iiasa.ac.at/RcpDb).

2.4. Forest expansion scenarios

Land use and land cover data for the contemporary period (2000–2019) was obtained from NLCD 2019. For the period of 2080–2099, we developed 11 forest expansion scenarios (FE0 to FE10) with variations in forest and grassland areas. For FE0, it is assumed that land use and land cover type during 2080–2099 remains the same as that in 2000–2019. For FE1 – FE10, it is assumed that 10%, 20%, 30%, 40%, 50%, 60%, 70%, 80%, 90%, and 100% of the current grasslands will be converted into forests during 2080–2099. We acknowledge that it is unlikely for the grasslands to be entirely converted to forests due to the limited resources (Sankaran et al., 2005). As our objective is to determine the variations in streamflow across a full spectrum of forest expansion, we kept the forest expansion scenarios with high-level increase in forest area.

As the encroachment of eastern redcedar is widely happening in Oklahoma grasslands (Wang et al., 2017), it is selected as the woody plant species that replaces grasslands in the ten forest expansion scenarios. To determine locations of redcedar encroachment in these scenarios, we simulated redcedar habitat suitability in the existing grassland areas using maximum entropy modeling (MaxEnt) (Elith et al., 2011; Phillips and Dudík, 2008). Habitat suitability in this study refers to the ability of a habitat to support the survival and growth of a plant. We collected training samples from the USDA Forest Inventory and Analysis (FIA) National Program and used climate conditions, topography, and soil texture and properties as the predictor variables to simulate the spatial pattern of habitat suitability in Oklahoma. The process to estimate redcedar habitat suitability is summarized in Text S1 and the detailed process can be found in our recent publication (Yang et al., 2024). Fig. S5 shows the spatial pattern of the suitability map, based on which we identified nine thresholds at the 10th, 20th, 30th, 40th, 50th, 60th, 70th, 80th, and 90th percentiles to separate the grassland grids into ten equal portions and replaced the selected grassland grids with evergreen forests in the respective forest expansion scenarios (Fig. S6). Finally, we used each of the 10 maps of land cover types to generate new HRU maps for SWAT + simulations in these forest expansion scenarios.

2.5. Calibration and validation

The LRW has two USGS river gauge stations to monitor Little River water quantity and quality. The first station, USGS 07230500, is located near Tecumseh, OK (35.17° N, 96.93° W) and situated right below Lake Thunderbird. Due to the influence of lake water use and dam operation on streamflow at this site, it is not used for model calibration in this study. Instead, the second gauge station, USGS 07231000, was located near Sasakwa, OK (34.97° N, 96.51° W) and close to the watershed outlet (Fig. 1). We used the monthly streamflow records at this station to calibrate SWAT + parameters and validate model performance.

The model calibration period extended from January 2002 to December 2014, and the validation period encompassed January 2015 to December 2021. We used three evaluation metrics recommended by Moriasi et al. (2007), i.e., the Nash-Sutcliffe Efficiency (NSE), Percent Bias (PBIAS), and the ratio of the root mean square error to the standard deviation of measured data (RSR), to assess model performance against the streamflow measurements obtained from the USGS gauge station. Prior to model calibration, SWAT+ was initially executed using the default parameter values. The simulated streamflow achieved an NSE value of 0.76, indicating a "very good" level of performance according to the rating criteria established by Moriasi et al. (2007). To further enhance the simulation results, an auto-calibration procedure was applied using the Dynamically Dimensioned Search (DDS) Algorithm (Tolson and Shoemaker, 2007) to calibrate ten model parameters (listed and explained in Table 1) that potentially affect the ecosystem water budget. These parameters were selected based on previous studies that aimed to enhance the performance of SWAT or SWAT+ in simulating streamflow (e.g. Arnold et al., 2012; Qiao et al., 2015). We assessed parameter sensitivity by examining the impact of a 20% increase and decrease in each of the 10 selected model parameters on the simulated streamflow (Fig. S7). This sensitivity test revealed that the magnitude of the simulated streamflow in the Little River is notably influenced by eight out of the ten parameters: canmx, alpha, cn2, epco, esco, K, perco, and revap_co. Particularly, cn2 and perco are the two most influential parameters. Despite the minimal effect of ovn and surlag on the magnitude of streamflow, they are anticipated to alter flow velocity, the time needed for runoff to reach river channels, etc. Hence, we included these two parameters in the model calibration process.

In the calibration process, the percentage change in the original parameter values was utilized to adjust the model parameters. For the DDS algorithm, we set the number of total iterations to 200 and the neighborhood perturbation size parameter to 0.2 and used NSE as the objective function. Text S2 provides a detailed description of the calibration process using the DDS algorithm. During the auto-calibration procedure, the best NSE improved with the number of iterations and eventually reached a value of 0.82 (Fig. S8). Table 1 provides the optimal values of the ten selected model parameters that were obtained through the calibration process.

Table 1
Calibrated biophysical and hydrological parameters for SWAT + simulations in the Little River Watershed.

Parameters	Changed percentage (%)	Description
canmx	12.4	The maximum amount of water that the canopy can hold when fully developed
alpha	−4.49	The baseflow recession constant
cn2	7.38	The Soil Conservation Service (SCS) Curve Number (CN)
epco	5.03	Plant uptake compensation factor
esco	1.36	Soil evaporation compensation factor
K	10.4	Soil saturated hydraulic conductivity
ovn	6.98	Manning's "n" value for overland flow
perco	14.69	Percolation coefficient
revap_co	−4.46	Groundwater "revap" coefficient.
Surlag	12.84	Surface runoff lag coefficient

Next, the calibrated parameters were employed to simulate streamflow dynamics from January 2002 to December 2021 (Fig. 2). In the model validation period (January 2015 to December 2021), the calibrated SWAT + model exhibited high performance. The NSE value was 0.93, suggesting a strong agreement between the simulated and observed monthly streamflow. PBIAS was −20.1%, indicating a slight overestimation of the streamflow by the model. RSR was 0.26, indicating a good precision of the model in capturing the variability of the observed streamflow. The calibrated parameters in Table 1 were used for all the HRUs and all the model simulations in this study.

In addition, we conducted tests to assess whether SWAT+ with calibrated parameter could well represent the daily variations in streamflow during 2002–2021 in the Little River Watershed (Fig. S9). The results indicate that SWAT + captured the daily variations in streamflow ($R^2 = 0.54$). The model also performed well in replicating baseflow during the relatively dry periods. Nevertheless, it is important to note that the peak flow simulated by SWAT+ was higher than the USGS measurements, which explains the negative PBIAS values in model calibration and validation (Fig. 2).

2.6. Water budget comparison between grasslands and forests

Woody plants, owing to their deeper root and higher foliage area, typically exhibit higher water use and ET rates compared to herbaceous plants (Adane et al., 2018; Sheil, 2018). The increase in forest coverage can result in a notable increase in global evapotranspiration (ET) (Wang et al., 2021) and affect water yield (Shi et al., 2011). To simulate the impact of land cover change on streamflow, it is necessary to have reasonable estimates of water budget in grasslands and forests. However, due to the absence of water flux and runoff measurements in the LRW, we gathered data from adjacent areas in other studies and subsequently made comparisons with SWAT + simulations.

Zou et al. (2014) investigated the alteration of hydrological processes caused by WPE in a mesic grassland watershed located ~90 km north of our study area and reported that the annual runoff coefficients during 2009–2011 were 10.6% in grassland watershed, compared to 2.1% in the WPE watershed. In the same three years, our SWAT + results showed an average runoff coefficient of 12% in the grassland HRUs and 3.7% in the forest HRUs in the LRW. Notably, SWAT + effectively captured the higher runoff coefficient in grasslands than that in forests as observed by Zou et al. (2014). It is also noteworthy that SWAT + simulated slightly higher runoff coefficients by 1.4–1.6% than Zou et al. (2014). These disparities could be attributed to differences in climate and vegetation conditions between the two watersheds.

Based on remote sensing observations, Wang et al. (2018b) found that land conversion from grasslands to juniper woodlands in Oklahoma could result in a substantial increase in ET by 30–55%. The ET differences between forests and grasslands have been confirmed by site observations (Duesterhaus, 2008). Our SWAT + simulations in the period of 2000–2019 indicated that annual ET in forest HRUs was 47% higher than in grassland HRUs (with values of 600 mm for grassland and 881 mm for forests), aligning with the results reported by Wang et al. (2018b). SWAT + simulations generally captured the distinct water budget variations between grasslands and forests. Therefore, our calibrated SWAT+ is suitable for quantifying the impacts of forest expansion on streamflow in the subhumid region.

2.7. Model experimental design and result analyses

In this study, a total of 121 SWAT + simulations were designed to simulate monthly streamflow dynamics at the beginning and end of the 21st century under various climate and forest expansion scenarios (Table S1). For the contemporary period of 2000–2019, 11 simulations (S1 – S11) were conducted with NLCD 2019 land cover data and climate conditions from gridMet and the five ESMs in the MACA v2 dataset. In the future period of 2080–2099, 110 simulations were designed to assess the impacts of climate change and land cover change on streamflow. These simulations were carried out using climate data from the five ESMs in the RCP45 and RCP85 scenarios and land cover data in eleven forest expansion scenarios (Fig. S6). In this study, we did not make model simulations for the middle century. SWAT + simulates forest water dynamics during the mature stage of forests. Given forest expansion and tree growth take time, it is unlikely for all trees to reach maturity by the middle of the century, Hence, we opted to conduct SWAT + future simulations for the period of 2080–2099.

The simulations of S2 – S11 and the simulations of S12 – S21 involved the use of the same land cover data but differed in climate data. Specifically, S2 – S11 simulations utilized MACA v2 climate data for the period of 2000–2019, while S12 – S21 simulations utilized MACA v2 climate data for the period of 2080–2019. Consequently, the disparity in streamflow between the two sets of simulations can be attributed to the effects of climate change between the early and end of the 21st century in the RCP45 and RCP85 scenarios. Additionally, the simulations of S12 – S21, S22 – S31, S32 – S41, S42 – S51, S52 – S61, S62 – S71, S72 – S81, S82 – S91, S92 – S101, S102 – S111, and S112 – S121 employed the same MACA v2 climate data for the period 2080–2099 but differed in the land

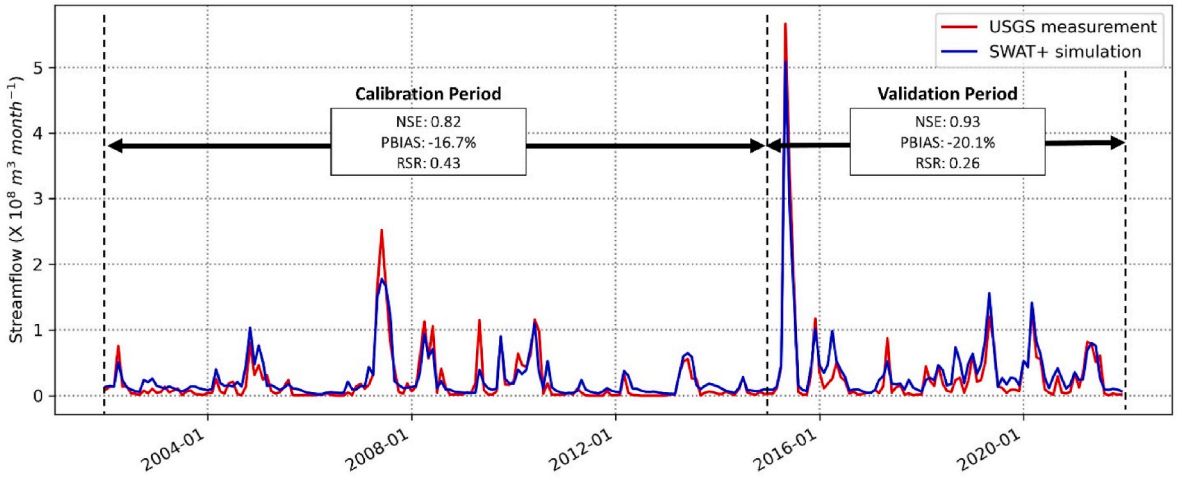

Fig. 2. Comparison of monthly streamflow ($\times 10^8$ m^3 $month^{-1}$) between SWAT + model simulation and measurements at USGS gauge station (ID: 07231000). Model calibration period was between January 2002 and December 2014 and the validation period was from January 2015 to December 2021. Three evaluation metrics were used to evaluate model performance, including Nash-Sutcliffe efficiency (NSE), percent bias (PBIAS), and ratio of the root mean square error to the standard deviation of measured data (RSR).

cover in the 11 forest expansion scenarios. Therefore, the variations between the 11 groups of simulations elucidate impacts of the increased woody plant area on streamflow.

Our analysis primarily focused on the streamflow at the watershed outlet. Additionally, we also considered the inflow into Lake Thunderbird, given its importance for understanding the long-term sustainability of water supply for the Oklahoma City metropolitan area in response to the changing climate conditions and land cover types.

3. Results

3.1. Climate change in the Little River Watershed

The LRW was projected to undergo significant climate change between the first and last 20-year periods of the 21st century, as outlined in Table 2. Based on the average climate data from the five ESMs, it is expected that the annual temperature in this region will increase from 17.3 °C to 19.4 °C in the RCP45 and from 17.2 °C to 22.3 °C in the RCP85. The increase in temperature is consistent across all the five ESMs, with projected temperature rises ranging from 1.5 °C to 2.6 °C for the RCP45 and from 3.8 °C to 6.1 °C for the RCP85.

According to the average of the five ESMs, the projected changes in precipitation for the LRW indicated contrasting trends between the RCP45 and the RCP85. Under the RCP45, the average annual precipitation was expected to increase slightly by 2.4%, from 1011 mm (25.6×10^8 m^3 $year^{-1}$) during 2000–2019 to 1035 mm (26.2×10^8 m^3 $year^{-1}$) during 2080–2099. Four out of the five ESMs projected an increase in annual precipitation, while one ESM (GFDL) showed a decrease. In contrast, the RCP85 scenario suggested a decline in average annual precipitation for the LRW. The average of the five ESMs indicated a decline of 7.1% from 1035 mm (26.2×10^8 m^3 $year^{-1}$) to 961 mm (24.3×10^8 m^3 $year^{-1}$). Four ESMs projected a decrease in annual precipitation, while one ESM (MIROC) showed an increase. Overall, these projections suggested that the LRW will experience a wetter climate in the RCP45 but a drier environment in the RCP85 by the end of the 21st century.

3.2. Changes in streamflow due to climate change

Climate change was projected to impose diverged impacts on streamflow at watershed outlet between the RCP45 and RCP85 scenarios (Fig. 3). During 2000–2019 in the RCP45, the average streamflow at the LRW outlet, simulated by SWAT + using climate data from the five ESMs, ranged from 3.84×10^8 m^3 $year^{-1}$ (IPSL) to 5.18×10^8 m^3 $year^{-1}$ (MIROC), with an average of 4.68×10^8 m^3 $year^{-1}$. In the last 20 years of the 21st century, the simulated streamflow in the RCP45 ranged from 4.04×10^8 m^3 $year^{-1}$ (GFDL) to 5.67×10^8 m^3 $year^{-1}$ (MIROC), with an average of 4.92×10^8 m^3 $year^{-1}$. In the RCP45, the annual average streamflow at the outlet was expected to increase by 0.24×10^8 m^3 $year^{-1}$ (5.1%) between the first and last 20 years of the 21st century. The increase in streamflow under the RCP45 can be attributed to the higher precipitation rate at the end of the 21st century (Table 2). However, it is worth noting that SWAT + also simulated a slight increase in annual evapotranspiration at the watershed scale, from 750 mm (19.0×10^8 m^3 $year^{-1}$) to 766 mm (19.4×10^8 m^3 $year^{-1}$). This increase in evapotranspiration was projected to partially offset the impact of increased precipitation on streamflow.

During 2000–2019 in the RCP85, the average streamflow simulated by SWAT + driven by climate data from the five ESMs ranged from 4.33 $\times 10^8$ m^3 $year^{-1}$ (MIROC) to 5.74×10^8 m^3 $year^{-1}$ (GFDL), with an overall average of 5.17×10^8 m^3 $year^{-1}$. During 2080–2099, the average streamflow simulated by SWAT + ranged from 3.26×10^8 m^3 $year^{-1}$ (IPSL) to 3.95×10^8 m^3 $year^{-1}$ (HadGEM), with an average of 3.61×10^8 m^3 $year^{-1}$. This suggested a notable decrease in annual streamflow of 1.56×10^8 m^3 $year^{-1}$ (30.1 %) at the watershed outlet between the first and last 20 years of the 21st century in the RCP85. Furthermore, the average annual evapotranspiration at the watershed level was projected to increase from 749 mm (18.9×10^8 m^3 $year^{-1}$) during 2000–2019 to 760 mm (19.2×10^8 m^3 $year^{-1}$) during 2080–2099. Therefore, the reduction in streamflow in the RCP85 can be attributed to both the decreased precipitation (Table 2) and increased evapotranspiration.

In the RCP45, monthly variations of the simulated streamflow in the period 2080–2099 were similar to those in 2000–2019 (Fig. 4). Between the two 20-year periods, streamflow was projected to show a decline of 8.9% between January and April but an increase of 22.9% between July and December. On the other hand, in the RCP85, all months were projected to experience a decrease in streamflow. The largest declines were in spring and early summer. Specifically, streamflow in March, April, May, and June was projected to decrease by 35.8%, 44.8%, 50.1%, and 42.3%, respectively, compared to the streamflow levels in the contemporary period. These changes in monthly streamflow patterns indicated the significant impacts of climate change on the seasonal pattern of streamflow in the LRW.

3.3. Changes in streamflow due to increased forest coverage

Our projections revealed a clear trend: as forest coverage increases, watershed ET would increase while streamflow would show a corresponding decrease, following a linear relationship under both the RCP45 and the RCP85 scenarios (Fig. 5). During the period of 2080–2099, if all the current grasslands are replaced by forests, annual ET is expected to increase by 95.6 mm (2.3×10^8 m^3 $year^{-1}$ or 12.5%) in the RCP45 and 70.7 mm (1.7×10^8 m^3 $year^{-1}$ or 9.3%) in the RCP85. Furthermore, each 10% grassland conversion to forests would lead to an incremental rise in watershed ET by 10.4 mm $year^{-1}$ (0.3×10^8 m^3 $year^{-1}$ or 1.3%) in the RCP45 and 7.5 mm $year^{-1}$ (0.2×10^8 m^3 $year^{-1}$ or 0.9%) in the RCP85. Conversely, if all grasslands are replaced by forests, the average simulated streamflow would decrease significantly by 41.1% from 4.92 $\times 10^8$ m^3 $year^{-1}$ to 2.9×10^8 m^3 $year^{-1}$ in the RCP45 and by 41% from 3.61×10^8 m^3 $year^{-1}$ to 2.13×10^8 m^3 $year^{-1}$ in the RCP85. Each 10% grassland conversion to forests would further reduce streamflow by 0.21×10^8 m^3 $year^{-1}$ (5.3 %) in the RCP45 and 0.16×10^8 m^3 $year^{-1}$ (5.3 %) in the RCP85. The decline in streamflow can be attributed

Table 2
Statistics of annual temperature and precipitation in the Little River Watershed in the two 20-year periods of 2000–2019 and 2080–2099. In the precipitation columns, values within the parentheses show the precipitation volume in the unit of $\times 10^8$ m^3 $year^{-1}$.

	Temperature (°C)				Precipitation (mm $year^{-1}$ or $\times 10^8$ m^3 $year^{-1}$)			
	RCP45		RCP85		RCP45		RCP85	
	2000–2019	*2080–2099*	*2000–2019*	*2080–2099*	*2000–2019*	*2080–2099*	*2000–2019*	*2080–2099*
bcc	17.1	18.6	17.1	21.6	1055 (26.7)	1086 (27.5)	1040 (26.3)	928 (23.5)
GFDL	16.7	18.4	16.8	20.6	1043 (26.4)	954 (24.1)	1057 (26.7)	950 (24.0)
HadGEM	17.6	20.2	17.6	22.7	982 (24.8)	1011 (25.6)	1047 (26.5)	1006 (25.4)
IPSL	17.6	19.7	17.3	23	958 (24.1)	1000 (25.3)	1049 (26.5)	928 (23.5)
MIROC	17.4	19.9	17.3	23.4	1017 (25.7)	1122 (28.4)	984 (24.9)	994 (25.1)
Average	17.3	19.4	17.2	22.3	1011 (25.6)	1035 (26.2)	1035 (26.2)	961 (24.3)

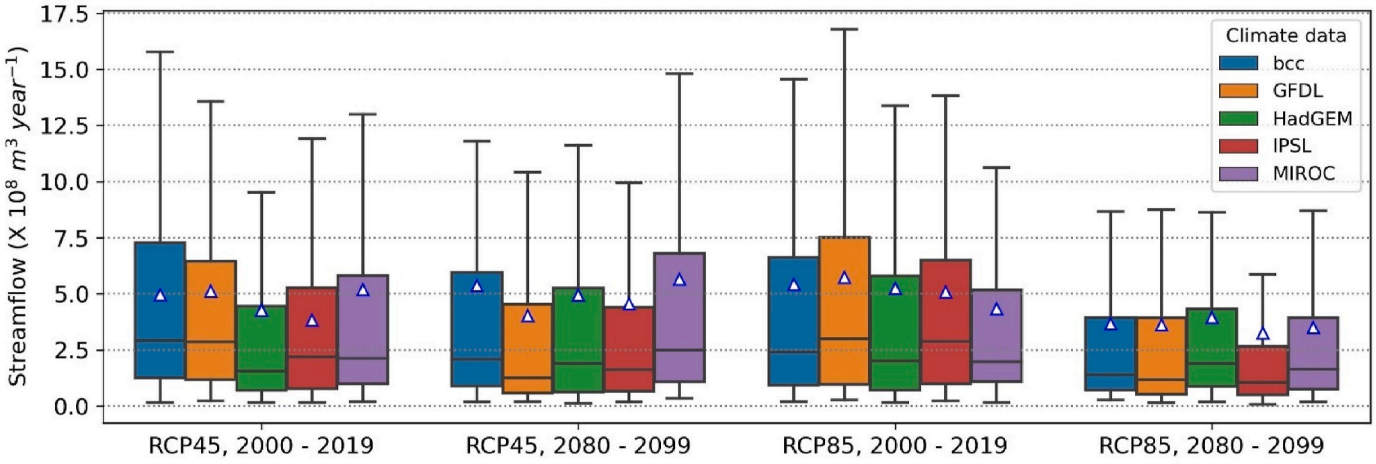

Fig. 3. Simulated annual streamflow ($\times 10^8$ m^3 $year^{-1}$) at the outlet of the Little River Watershed simulated by SWAT+ in the two 20-year periods of 2000–2019 and 2080–2099 under the RCP45 and RCP85 scenarios. SWAT+ was driven by climate data from five Earth System Models, including bcc, GFDL, HadGEM, IPSL, and MIROC. The box plot presents streamflow variations in the 20-year simulation period. The triangles show the average of the 20-year streamflow.

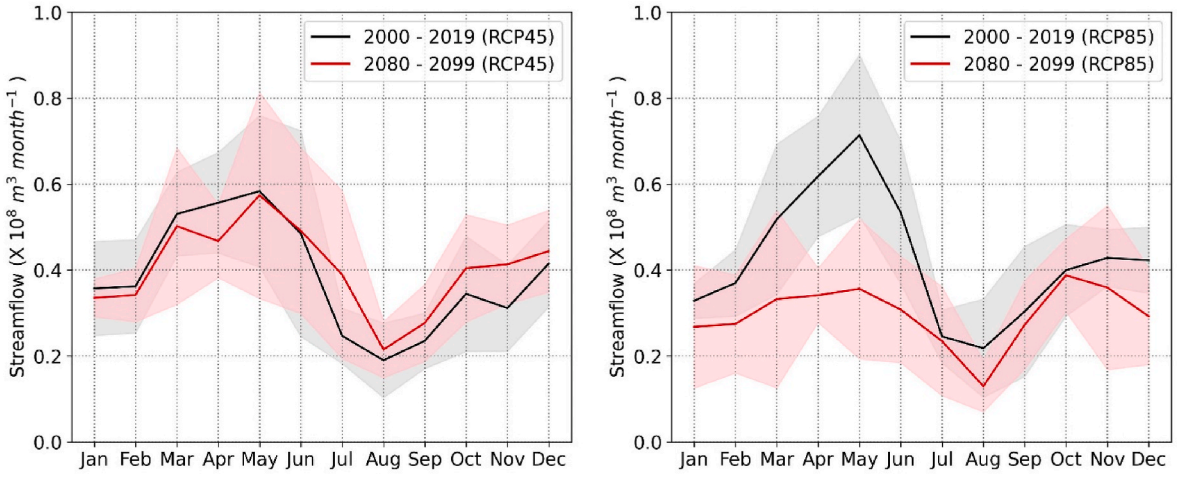

Fig. 4. Average monthly streamflow ($\times 10^8$ m^3 $month^{-1}$) of the Little River Watershed simulated by SWAT+ in the 20-year periods of 2000–2019 and 2080–2099 under the RCP45 (left) and RCP85 (right). SWAT+ was driven by climate data from five Earth System Models, including bcc, GFDL, HadGEM, IPSL, and MIROC. The gray and pink shaded areas show the ±1 standard deviation of the simulation results driven by climate data from five Earth System Models.

primarily to the increase in evapotranspiration.

We further evaluated the decrease in streamflow during the wet, normal, and dry years caused by forest expansion in the period of 2080–2099 (Fig. 6). Wet years, normal years, and dry years were defined based on annual precipitation: wet years refer to the years with annual precipitation greater than the 90th percentile, dry years refer to the years with annual precipitation less than the 10th percentile, and normal years refer to the years with annual precipitation between the 10th and the 90th percentiles (Pan et al., 2020). Results show that, if all grasslands were replaced by forests in the RCP45 scenario, average streamflow would decrease by 4.8 $\times 10^8$ m^3 $year^{-1}$ (37.4%) from 12.9 $\times 10^8$ m^3 $year^{-1}$ to 8.1 $\times 10^8$ m^3 $year^{-1}$ in the wet years, by 1.8 $\times 10^8$ m^3 $year^{-1}$ (42.4%) from 4.3 $\times 10^8$ m^3 $year^{-1}$ to 3.5 $\times 10^8$ m^3 $year^{-1}$ in the normal years, and by 0.7 $\times 10^8$ m^3 $year^{-1}$ (41.4%) from 1.7 $\times 10^8$ m^3 $year^{-1}$ to 1.0 $\times 10^8$ m^3 $year^{-1}$ in the dry years. Additionally, if all grasslands were replaced by forests in the RCP85 scenarios, average streamflow would decrease by 4.3 $\times 10^8$ m^3 $year^{-1}$ (43.1%) from 9.9 $\times 10^8$ m^3 $year^{-1}$ to 5.6 $\times 10^8$ m^3 $year^{-1}$ in the wet years, by 1.3 $\times 10^8$ m^3 $year^{-1}$ (40.3%) from 3.1 $\times 10^8$ m^3 $year^{-1}$ to 1.9 $\times 10^8$ m^3 $year^{-1}$ in the normal years, and by 0.4 $\times 10^8$ m^3 $year^{-1}$ (33.0%) from 1.1 $\times 10^8$ m^3 $year^{-1}$ to 0.8 $\times 10^8$ m^3 $year^{-1}$ in the dry years.

3.4. Water inflow to Lake Thunderbird

Based on simulation S1, the average water inflow into Lake Thunderbird during 2000–2019 was 0.98 $\times 10^8$ m^3 $year^{-1}$, exhibiting significant monthly and interannual variations (Fig. 7). Among the years analyzed, the highest annual inflows were observed in 2007 (2.24 $\times 10^8$ m^3 $year^{-1}$) and 2015 (3.16 $\times 10^8$ m^3 $year^{-1}$). Conversely, the lowest annual inflows were in 2003 (0.39 $\times 10^8$ m^3 $year^{-1}$), 2006 (0.36 $\times 10^8$ m^3 $year^{-1}$), 2011 (0.5 $\times 10^8$ m^3 $year^{-1}$), 2012 (0.49 $\times 10^8$ m^3 $year^{-1}$), and 2014 (0.43 $\times 10^8$ m^3 $year^{-1}$). At the monthly scale, the highest inflows into Lake Thunderbird were in early summer. Specifically, May and June exhibited inflow rates of 19.5 $\times 10^6$ m^3 $month^{-1}$ and 13.6 $\times 10^6$ m^3 $month^{-1}$, respectively. On the other hand, the lowest inflows occurred in winter months, with December, January, and February recording rates of 4.4 $\times 10^6$ m^3 $month^{-1}$, 3.8 $\times 10^6$ m^3 $month^{-1}$, 4.1 $\times 10^6$ m^3 $month^{-1}$, respectively.

According to the average of SWAT + simulations driven by climate data from five ESMs, the water inflow into Lake Thunderbird would exhibit different trends under the RCP45 and the RCP85, consistent with the simulated streamflow at the watershed outlet. In the RCP45 scenario, future climate change was anticipated to result in an increase in

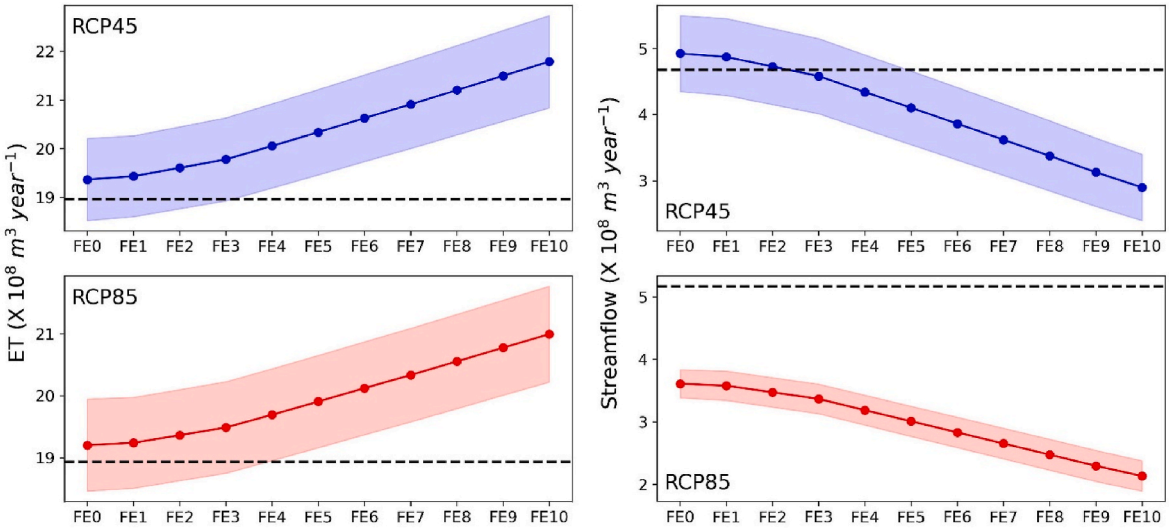

Fig. 5. The simulated annual average evapotranspiration (ET, $\times 10^8$ m^3 year^{-1}) in the Little River Watershed and streamflow ($\times 10^8$ m^3 year^{-1}) at the outlet during 2080–2099 under 11 forest expansion scenarios (FE0 – FE10) and two climate scenarios of the RCP45 and the RCP85. The shade area shows the ±1 standard deviation of the simulation results driven by climate data from five Earth System Models. Dash lines denote the level of average ET or streamflow during 2000–2019 in the RCP45 and the RCP85 scenarios.

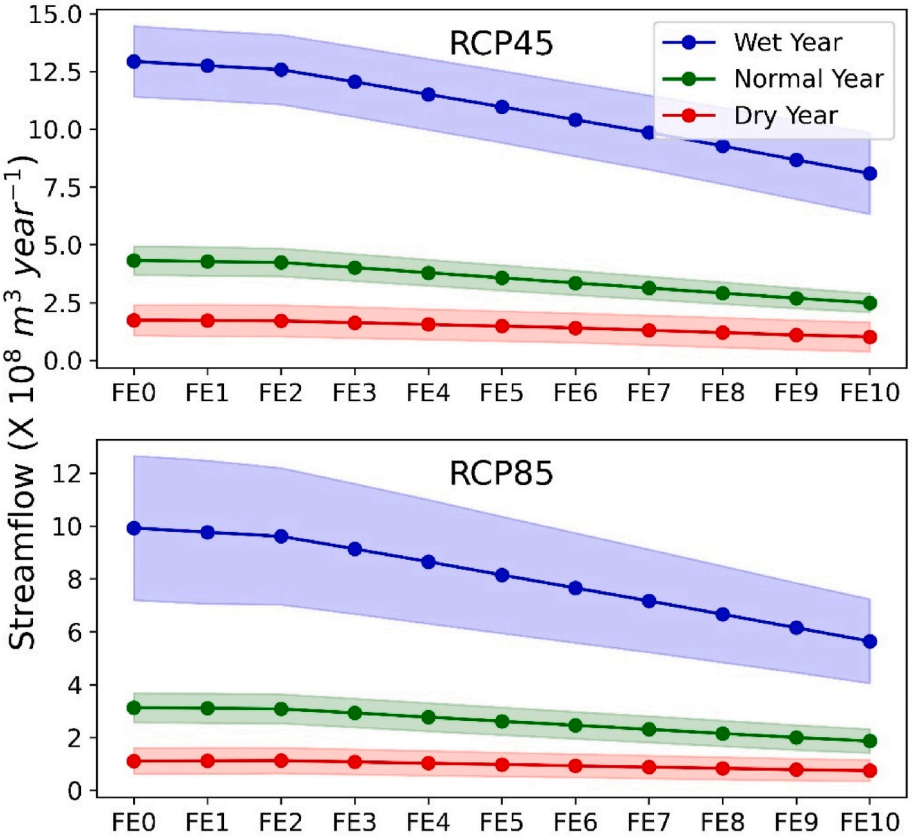

Fig. 6. The changes in streamflow ($\times 10^8$ m^3 year^{-1}) with forest expansion under 11 forest expansion scenarios (FE0 – FE10) in the wet (blue), normal (green), and dry (red) years. Streamflow was simulated at the outlet of the Little River Watershed during 2080–2099 under two climate scenarios of the RCP45 and the RCP85. The shade area shows the ±1 standard deviation of the simulation results driven by climate data from five Earth System Models.

water inflow by 3.6% from 1.1 $\times 10^8$ m^3 year^{-1} during the period of 2000–2019 to 1.14 $\times 10^8$ m^3 year^{-1} during the period of 2080–2099. Climate change under the RCP85 scenario was expected to reduce water inflow into Lake Thunderbird by 24.8% from 1.21 $\times 10^8$ m^3 year^{-1} during the period of 2000–2019 to 0.91 $\times 10^8$ m^3 year^{-1} during the period of 2080–2099.

The conversion of grassland to forest is anticipated to lead to a considerable reduction in water inflow into Lake Thunderbird, impacting future water availability for the Oklahoma City metropolitan area. We conducted a comparative analysis of the simulated annual water

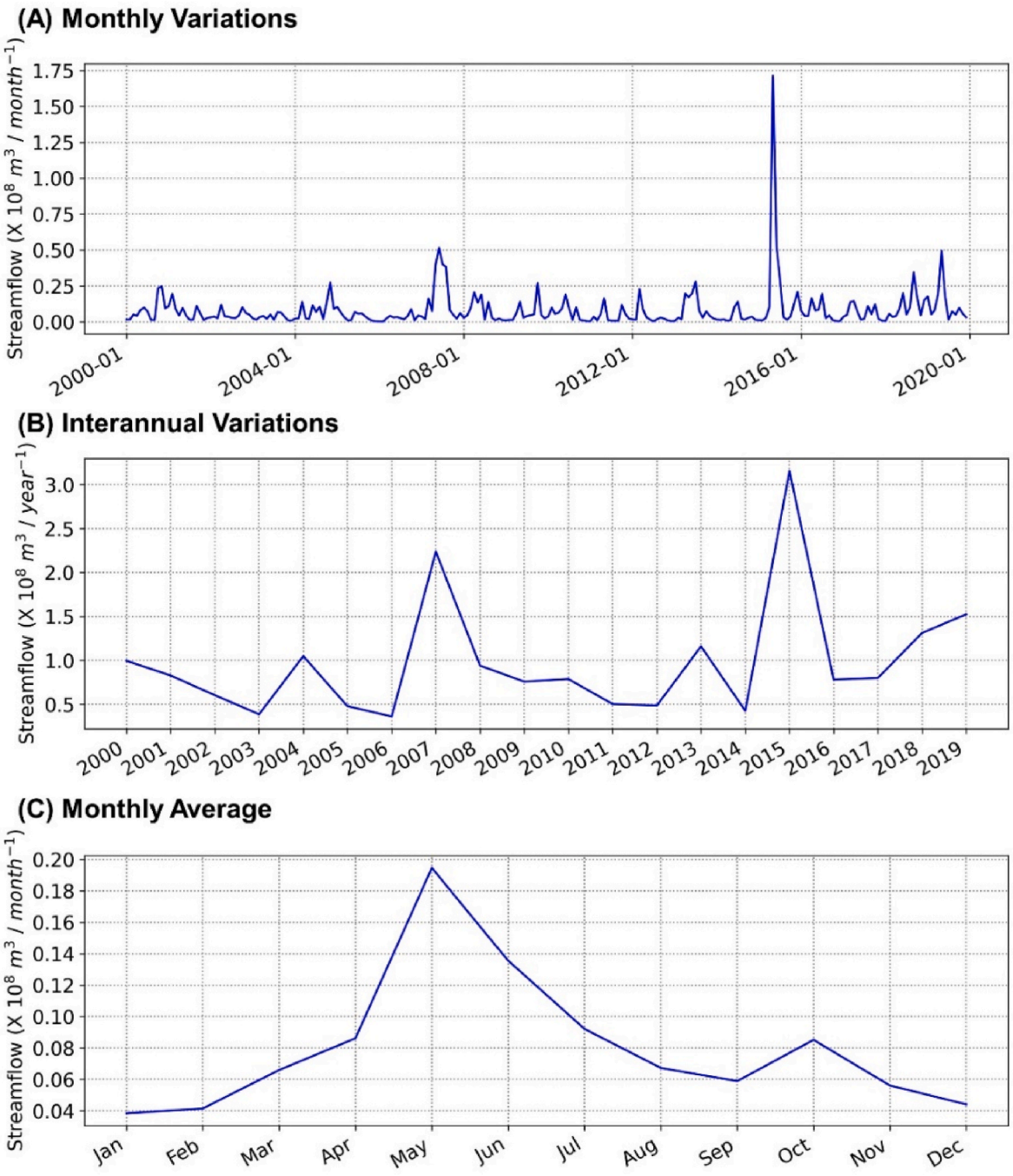

Fig. 7. Water inflow into Lake Thunderbird during 2000–2019, simulated by SWAT + driven by gridMET climate data. (A) Monthly variations ($\times 10^8$ m^3 $month^{-1}$), (B) interannual variations ($\times 10^8$ m^3 $year^{-1}$), and (C) monthly average ($\times 10^8$ m^3 $month^{-1}$).

inflow into Lake Thunderbird across the 11 forest expansion scenarios (FE0 – FE10) during 2080–2099 with the water inflow in the two extremely dry years 2011 and 2012 (0.49×10^8 m^3 $year^{-1}$). In these two years, the lake water level was 2.1 m below the recommended conservation pool (Fig. 8). The results indicated that under the scenario of no forest expansion (FE0), there would be an average of 5.4 years in the RCP45 and 6.6 years in the RCP85 during 2080–2099 with lower water inflow into Lake Thunderbird than the rates experienced during 2011/2012. When 50% of the grasslands are converted into forests (FE5), the duration would extend to 6.8 years for both the RCP45 and RCP85. In the scenario that all grasslands are replaced by forests (FE10), an average of 8.6 years and 9.4 years would experience a low water inflow into Lake Thunderbird in the RCP45 and the RCP85, respectively.

4. Discussion

4.1. Water resources availability under climate change

Climate change plays a significant role in altering river flows and has substantial implications for future water resources (Döll and Schmied, 2012). In the United States, Caldwell et al. (2012) used an water balance and flow routing model to project future river flow and found a 16% decrease in mean annual river flows in the 2060s compared to the 2010s, highlighting the impact of climate change on surface water availability at the national level. In the LRW, our simulations showed that by the end of the 21st century, streamflow will experience a slight increase of 5.1% in the RCP45 due to increased precipitation. However, in the RCP85,

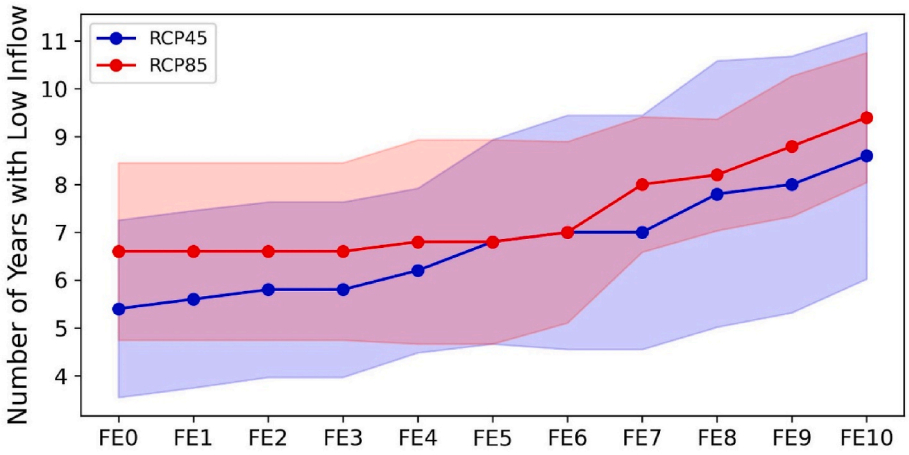

Fig. 8. Number of years with low annual water inflow into Lake Thunderbird during 2080–2099 in the 11 forest expansion scenarios (FE0 – FE10). The threshold to define low annual water inflow is the inflow amount in 2011 and 2012. The shaded area shows the ±1 standard deviation of SWAT + simulation results driven by climate data from five Earth System Models.

streamflow was projected to significantly decrease by 30.1 % as a result of reduced precipitation and enhanced evapotranspiration. Notably, the decline was projected to be particularly pronounced during spring and early summer. As spring is the season with the highest precipitation and streamflow in the subhumid region in the United States, water storage in reservoirs is replenished by streamflow in this season. The projected decline in spring streamflow can significantly reduce water storage in reservoirs in central United States and limit the sustainable water supply under the RCP85 climate scenarios. Noted that the decrease in seasonal streamflow does not necessarily indicate a lower flood risk. It is possible that future climate change reduces annual and seasonal precipitation while enhancing the likelihood of extreme precipitation events and consequent flooding (Tabari, 2020).

Although climates projected by different ESMs showed considerable divergence, the average results in the RCP45 scenario demonstrated a slight increase in streamflow, offering potential support for a sustainable water supply in the central United States. Presently, numerous climate change mitigation strategies are being investigated or implemented in countries with substantial carbon emissions, such as the United States, China, and the European Union (Chen et al., 2022). These mitigation strategies encompass various approaches, including but not limited to renewable energy production (Hanssen et al., 2020), transport electrification (Zhang and Fujimori, 2020), and reforestation (Silver et al., 2000). Implementing these strategies has the potential to deviate future climate change from the trajectory of the RCP85 scenario, consequently improving water resource availability in the central United States.

4.2. Global implications for afforestation

Our simulations demonstrated that land conversion from grasslands to forests would have large impacts on evapotranspiration and subsequent streamflow, which is applicable to the broader subhumid region at the global level. If all grasslands were to be replaced by forests, streamflow in the LRW was projected to decrease by 41% compared to the scenario without land cover change. Additionally, over the 20-year period of 2080–2099, Lake Thunderbird would experience an average of 8.6 years in the RCP45 and 9.4 years in the RCP85 with water inflow amounts lower than those during the 2011/2012 extreme drought event. These results emphasize that forest expansion due to afforestation or WPE can substantially diminish water resources sustainability in the subhumid ecoregion irrespective of the climate change scenarios. While afforestation/reforestation efforts in the subhumid region offer numerous ecological benefits, it is crucial to approach afforestation strategies with careful consideration of the potential decline in water availability, particularly in watersheds critical for municipal water supply.

The impact of afforestation on surface runoff varies significantly across different climate zones, with estimates indicating a reduction from 54% in drier areas to less than 15% in more humid areas (Trabucco et al., 2008). Moreover, studies suggest that afforestation in humid areas might have a modest effect on groundwater storage (Ouyang et al., 2021). When considering water resource management, implementing large-scale afforestation appears more suitable for humid regions. However, it is important to note that afforestation has been implemented across the global subhumid and dryland areas, which was observed to increase ecosystem water consumption. Consequently, implementation of afforestation in subhumid and dryland areas necessitates meticulous planning, accounting for factors such as heightened ET with tree cover, the response of dryland forests to future climate change, and their potential socioeconomic impacts (Liu et al., 2022).

4.3. Potential management strategies to control woody plant encroachment

A variety of management strategies have been employed to curb the spread of woody species in grasslands. Herbicide injection, initiated in the 1960s, has been used to eliminate woody plants (Archer and Predick, 2014). However, this method is labor-intensive and offers relatively short-term effectiveness of less than 10 years (Scholtz et al., 2021). Another way to control redcedar spread involves mechanical removal. This is a common practice for quickly reclaiming the encroached land (Morton et al., 2010). However, mechanical treatment can be costly, ranging from $25 and $100 per acre depending on tree size and density. Currently, the most effective strategy for controlling redcedar encroachment is probably the implementation of prescribed fires (Wilcox et al., 2018). Given the fact that eastern redcedar is highly intolerant to fires (Jeffries et al., 2023), prescribed burns can effectively eliminate redcedar seedlings in grasslands. Redcedar trees with a height up to 4.5 m can be eliminated when fire intensity reaches 160 kJ m^{-1} s^{-1} (Twidwell et al., 2013).

4.4. Uncertainties and future research needs

SWAT + demonstrated excellent performance in simulating the monthly variations of streamflow in the LRW, as evidenced by the high NSE of 0.93 in the model validation period. Moreover, SWAT + simulated a higher ET in forests compared to grasslands, aligning with previous field measurements and remote sensing results. This indicated that SWAT + can successfully capture streamflow dynamics under diverse climate conditions and land conversion scenarios. However, in this

study, SWAT + overestimated the peak flow to a certain degree. Additionally, it is important to note that future climate data generated from ESMs introduced considerable uncertainties in river flow simulations (Prudhomme and Davies, 2009; van Vliet et al., 2013). In this study, we utilized future climate data from five ESMs to drive the SWAT+ and showed the ensemble mean and range of simulated streamflow to represent the uncertainty associated with future climate projections.

Future climate change is accompanied by rising CO_2 concentration, which modifies land hydrological processes through its effects on vegetation biophysical and physiological conditions (Piao et al., 2007; Shi et al., 2011; Yang et al., 2023). The current version of SWAT + allowed us to specify a fixed CO_2 concentration in each 20-year simulation period. Recent studies indicated that incorporating interannual variations in CO_2 input instead of a fixed value can lead to different patterns of evapotranspiration and river flow (Wu et al., 2012; Zhang et al., 2022). Therefore, the inclusion of annual CO_2 input data could be a necessary step for the improvement of SWAT + to reduce the uncertainties in streamflow projections under future climate conditions.

Another source of uncertainty in SWAT + emerges from its handling of tree growth. Being a hydrological model, SWAT + primarily simulates forest hydrological processes at a mature stage. However, it is widely acknowledged that ecosystem ET and other water processes vary significantly with forest conditions and canopy coverage (Cornish and Vertessy, 2001). Therefore, the accuracy of SWAT+'s estimation for ET and runoff could be less reliable for young forests in their early growth stage.

Ecosystems within the subhumid region exhibit a high sensitivity to both climate variations and long-term climate change (Knapp et al., 1998). Understanding hydrological processes in forests and grasslands as well as the distinctions between these ecosystems in the subhumid region is vital for modeling regional water availability under the shifting composition of ecosystems and changing future climate conditions. Considering this, we suggest the installation of sufficient eddy covariance flux towers, soil moisture probes, and H flumes in paired forest and grassland experimental watersheds in forest-grassland transition zone. This expanded data collection effort will significantly contribute to refining hydrological models and enhancing the projection accuracy of regional water availability.

Our study focused on the examination of streamflow variations under climate change and forest expansion. Baseflow, integral to streamflow, sustains minimum water supply during dry seasons and droughts (Lee and Ajami, 2023). In dry areas, changes in forest coverage might have a dual impact on groundwater recharge and baseflow (Acharya et al., 2018). For example, Wilcox (2002) discovered that the reduction in woodland area could augment groundwater recharge, while Ilstedt et al. (2016) noted that increased tree cover could enhance groundwater recharge and baseflow. Our study did not specifically analyze the changes in baseflow with forest expansion. We conducted a preliminary analysis to compare monthly streamflow between FE0 and FE10 (Fig. S10). The result showed that forest expansion could slightly reduce streamflow during the dry period, indicating a small but negative impact of forest expansion on baseflow in the Little River Watershed. Additional research is still needed to comprehend how forest expansion influences baseflow variations under future climate conditions in subhumid regions.

5. Conclusions

In this study, we utilized the SWAT + to simulate the monthly variations of streamflow in the Little River Watershed and water inflow into Lake Thunderbird, considering both present and future climate conditions, as well as eleven forest expansion scenarios. Our findings provided valuable insights into the potential impacts of future climate change and the expansion of forest coverage on water resources in the subhumid region. First, our results indicated that, driven by climate data from multiple ESMs, average annual streamflow in the Little River Watershed will increase by 5.1% in the RCP45 but decrease by 30.1% in the RCP85. The decline in streamflow in the RCP85 was projected to be particularly pronounced in the spring and early summer months. Furthermore, our simulations demonstrated a linear decrease in streamflow corresponding to increases in forest coverage. If all grasslands are replaced by forests, streamflow would decrease by additional 41% and Lake Thunderbird is anticipated to experience an average of 8.6 years in the RCP45 and 9.4 years in the RCP85 during the 20-year period of 2080–2099 with water inflow amounts lower than those in the 2011/2012 extreme drought event. These findings underscore the severe consequences of forest expansion on future water resource availability. Therefore, the formulation of afforestation/reforestation policies in the subhumid region and the implementation of WPE management practices necessitate a comprehensive evaluation of their long-term impacts on water resources sustainability.

CRediT authorship contribution statement

Jia Yang: Writing – review & editing, Writing – original draft, Methodology, Investigation, Data curation, Conceptualization. **Abigail Winrich:** Writing – review & editing, Writing – original draft, Methodology, Investigation. **Tian Zhang:** Methodology, Investigation. **Lei Qiao:** Methodology, Investigation. **Chris Mattingly:** Validation, Methodology, Investigation. **Chris Zou:** Writing – review & editing, Writing – original draft, Investigation, Funding acquisition, Conceptualization.

Declaration of competing interest

The authors declare that they have no known competing financial interests or personal relationships that could have appeared to influence the work reported in this paper.

Data availability

Data will be made available on request.

Acknowledgement

This work was supported by the Oklahoma NSF EPSCoR S3OK project (award number: OIA-1946093), S3OK project Research Seed Grant, USDA McIntire-Stennis Grant (OKL03249, OKL03151), and USDA Forest Service Agreement (21-JV-11330170-026). The authors would like to express their gratitude to Ms. Nancy Sammons for her assistance in providing the latest SWAT+ and technical support for the model simulations. The Authors declare that there are no conflicts of interests.

Appendix A. Supplementary data

Supplementary data to this article can be found online at https://doi.org/10.1016/j.jenvman.2024.120780.

References

Abatzoglou, J.T., 2013. Development of gridded surface meteorological data for ecological applications and modelling. Int. J. Climatol. 33, 121–131. https://doi.org/10.1002/joc.3413.

Abatzoglou, J.T., Brown, T.J., 2012. A comparison of statistical downscaling methods suited for wildfire applications. Int. J. Climatol. 32, 772–780. https://doi.org/10.1002/joc.2312.

Acharya, B.S., Hao, Y., Ochsner, T.E., Zou, C.B., 2017. Woody plant encroachment alters soil hydrological properties and reduces downward flux of water in tallgrass prairie. Plant Soil 414, 379–391. https://doi.org/10.1007/s11104-016-3138-0.

Acharya, B.S., Kharel, G., Zou, C.B., Wilcox, B.P., Halihan, T., 2018. Woody plant encroachment impacts on groundwater recharge: a review. Water 10, 1466. https://doi.org/10.3390/w10101466.

Adane, Z.A., Nasta, P., Zlotnik, V., Wedin, D., 2018. Impact of grassland conversion to forest on groundwater recharge in the Nebraska Sand Hills. J. Hydrol.: Reg. Stud. 15, 171–183. https://doi.org/10.1016/j.ejrh.2018.01.001.

Alkama, R., Cescatti, A., 2016. Biophysical climate impacts of recent changes in global forest cover. Science 351, 600–604. https://doi.org/10.1126/science.aac8083.
Ansley, R.J., Rivera-Monroy, V.H., Griffis-Kyle, K., Hoagland, B., Emert, A., Fagin, T., Loss, S.R., McCarthy, H.R., Smith, N.G., Waring, E.F., 2023. Assessing impacts of climate change on selected foundation species and ecosystem services in the South-Central USA. Ecosphere 14, e4412. https://doi.org/10.1002/ecs2.4412.
Archer, S., Andersen, E., Predick, K., Schwinning, S., Steidl, R., Woods, S., 2017. Chapter 2 woody plant encroachment: causes and consequences. In: Rangeland Systems. Springer, pp. 25–84.
Archer, S.R., Predick, K.I., 2014. An ecosystem services perspective on brush management: research priorities for competing land-use objectives. J. Ecol. 102, 1394–1407. https://doi.org/10.1111/1365-2745.12314.
Arnold, J.G., Moriasi, D.N., Gassman, P.W., Abbaspour, K.C., White, M.J., Srinivasan, R., Santhi, C., Harmel, R.D., Van Griensven, A., Van Liew, M.W., Kannan, N., Jha, M.K., 2012. SWAT: model use, calibration, and validation. Transactions of the ASABE 55, 1491–1508.
Bailey, R.T., Park, S., Bieger, K., Arnold, J.G., Allen, P.M., 2020. Enhancing SWAT+ simulation of groundwater flow and groundwater-surface water interactions using MODFLOW routines. Environ. Model. Software 126, 104660. https://doi.org/10.1016/j.envsoft.2020.104660.
Barger, N.N., Archer, S.R., Campbell, J.L., Huang, C., Morton, J.A., Knapp, A.K., 2011. Woody plant proliferation in North American drylands: a synthesis of impacts on ecosystem carbon balance. J. Geophys. Res.: Biogeosciences 116. https://doi.org/10.1029/2010JG001506.
Bastin, J.-F., Finegold, Y., Garcia, C., Mollicone, D., Rezende, M., Routh, D., Zohner, C. M., Crowther, T.W., 2019. The global tree restoration potential. Science 365, 76–79. https://doi.org/10.1126/science.aax0848.
Bieger, K., Arnold, J.G., Rathjens, H., White, M.J., Bosch, D.D., Allen, P.M., Volk, M., Srinivasan, R., 2017. Introduction to SWAT+, A completely restructured version of the soil and water assessment Tool. JAWRA Journal of the American Water Resources Association 53, 115–130. https://doi.org/10.1111/1752-1688.12482.
Briggs, J.M., Knapp, A.K., Blair, J.M., Heisler, J.L., Hoch, G.A., Lett, M.S., McCarron, J.K., 2005. An ecosystem in transition: causes and consequences of the conversion of mesic grassland to shrubland. Bioscience 55, 243–254. https://doi.org/10.1641/0006-3568(2005)055[0243:AEITCA]2.0.CO;2.
Caldwell, P.V., Sun, G., McNulty, S.G., Cohen, E.C., Moore Myers, J.A., 2012. Impacts of impervious cover, water withdrawals, and climate change on river flows in the conterminous US. Hydrol. Earth Syst. Sci. 16, 2839–2857. https://doi.org/10.5194/hess-16-2839-2012.
Canadell, J.G., Raupach, M.R., 2008. Managing forests for climate change mitigation. Science 320, 1456–1457. https://doi.org/10.1126/science.1155458.
Cerasoli, S., Yin, J., Porporato, A., 2021. Cloud Cooling Effects of Afforestation and Reforestation at Midlatitudes, vol. 118. Proceedings of the National Academy of Sciences, e2026241118. https://doi.org/10.1073/pnas.2026241118.
Chawanda, C.J., Arnold, J., Thiery, W., van Griensven, A., 2020. Mass balance calibration and reservoir representations for large-scale hydrological impact studies using SWAT+. Climatic Change 163, 1307–1327. https://doi.org/10.1007/s10584-020-02924-x.
Chen, J., Xu, C., Gao, M., Li, D., 2022. Carbon peak and its mitigation implications for China in the post-pandemic era. Sci. Rep. 12, 3473. https://doi.org/10.1038/s41598-022-07283-4.
Christian, J.I., Basara, J.B., Otkin, J.A., Hunt, E.D., Wakefield, R.A., Flanagan, P.X., Xiao, X., 2019. A methodology for flash drought identification: application of flash drought frequency across the United States. J. Hydrometeorol. 20, 833–846. https://doi.org/10.1175/JHM-D-18-0198.1.
Cornish, P.M., Vertessy, R.A., 2001. Forest age-induced changes in evapotranspiration and water yield in a eucalypt forest. J. Hydrol. 242, 43–63. https://doi.org/10.1016/S0022-1694(00)00384-X.
DeSantis, R.D., Hallgren, S.W., Stahle, D.W., 2011. Drought and fire suppression lead to rapid forest composition change in a forest-prairie ecotone. For. Ecol. Manag. 261, 1833–1840. https://doi.org/10.1016/j.foreco.2011.02.006.
Döll, P., Schmied, H.M., 2012. How is the impact of climate change on river flow regimes related to the impact on mean annual runoff? A global-scale analysis. Environ. Res. Lett. 7, 014037 https://doi.org/10.1088/1748-9326/7/1/014037.
Duesterhaus, J.L., 2008. A Micrometeorology Study of Stock Watering Ponds, Rangelands, and Woodlands in the Flint Hills of Kansas. Kansas State University.
Elith, J., Phillips, S.J., Hastie, T., Dudík, M., Chee, Y.E., Yates, C.J., 2011. A statistical explanation of MaxEnt for ecologists. Divers. Distrib. 17, 43–57. https://doi.org/10.1111/j.1472-4642.2010.00725.x.
FAO, 2022. The State of the World's Forests 2022. Forest Pathways for Green Recovery and Building Inclusive, Resilient and Sustainable Economies.
Griscom, B.W., Adams, J., Ellis, P.W., Houghton, R.A., Lomax, G., Miteva, D.A., Schlesinger, W.H., Shoch, D., Siikamäki, J.V., Smith, P., Woodbury, P., Zganjar, C., Blackman, A., Campari, J., Conant, R.T., Delgado, C., Elias, P., Gopalakrishna, T., Hamsik, M.R., Herrero, M., Kiesecker, J., Landis, E., Laestadius, L., Leavitt, S.M., Minnemeyer, S., Polasky, S., Potapov, P., Putz, F.E., Sanderman, J., Silvius, M., Wollenberg, E., Fargione, J., 2017. Natural climate solutions. Proc. Natl. Acad. Sci. USA 114, 11645–11650. https://doi.org/10.1073/pnas.1710465114.
Hansen, M.C., Potapov, P.V., Moore, R., Hancher, M., Turubanova, S.A., Tyukavina, A., Thau, D., Stehman, S.V., Goetz, S.J., Loveland, T.R., Kommareddy, A., Egorov, A., Chini, L., Justice, C.O., Townshend, J.R.G., 2013. High-resolution global maps of 21st-century forest cover change. Science 342, 850–853. https://doi.org/10.1126/science.1244693.
Hanssen, S.V., Daioglou, V., Steinmann, Z.J.N., Doelman, J.C., Van Vuuren, D.P., Huijbregts, M.a.J., 2020. The climate change mitigation potential of bioenergy with carbon capture and storage. Nat. Clim. Change 10, 1023–1029. https://doi.org/10.1038/s41558-020-0885-y.
Harris, N.L., Gibbs, D.A., Baccini, A., Birdsey, R.A., de Bruin, S., Farina, M., Fatoyinbo, L., Hansen, M.C., Herold, M., Houghton, R.A., Potapov, P.V., Suarez, D.R., Roman-Cuesta, R.M., Saatchi, S.S., Slay, C.M., Turubanova, S.A., Tyukavina, A., 2021. Global maps of twenty-first century forest carbon fluxes. Nat. Clim. Change 11, 234–240. https://doi.org/10.1038/s41558-020-00976-6.
Hoff, D.L., Will, R.E., Zou, C.B., Lillie, N.D., 2018. Encroachment dynamics of Juniperus virginiana L. And mesic hardwood species into Cross timbers forests of north-central Oklahoma, USA. Forests 9, 75. https://doi.org/10.3390/f9020075.
Homer, C.H., Fry, J.A., Barnes, C.A., 2012. The national land cover database. US geological survey fact sheet 3020, 1–4.
Huxman, T.E., Wilcox, B.P., Breshears, D.D., Scott, R.L., Snyder, K.A., Small, E.E., Hultine, K., Pockman, W.T., Jackson, R.B., 2005. Ecohydrological implications of woody plant encroachment. Ecology 86, 308–319. https://doi.org/10.1890/03-0583.
Ilstedt, U., Bargués Tobella, A., Bazié, H.R., Bayala, J., Verbeeten, E., Nyberg, G., Sanou, J., Benegas, L., Murdiyarso, D., Laudon, H., Sheil, D., Malmer, A., 2016. Intermediate tree cover can maximize groundwater recharge in the seasonally dry tropics. Sci. Rep. 6, 21930 https://doi.org/10.1038/srep21930.
Jeffries, K., Mishra, B., Russell, A., Joshi, O., 2023. Exploring opinions for using prescribed fire to control eastern redcedar (Juniperus virginiana) encroachment in the southern Great Plains, United States. Rangel. Ecol. Manag. 86, 73–79. https://doi.org/10.1016/j.rama.2022.10.002.
Joshi, O., Will, R.E., Zou, C.B., Kharel, G., 2019. Sustaining cross-timbers forest resources: current knowledge and future research needs. Sustainability 11, 4703. https://doi.org/10.3390/su11174703.
Karki, L., Hallgren, S.W., 2015. Tree-fall gaps and regeneration in old-growth Cross timbers forests. naar 35, 533–541. https://doi.org/10.3375/043.035.0405.
Kiprotich, P., Wei, X., Zhang, Z., Ngigi, T., Qiu, F., Wang, L., 2021. Assessing the impact of land use and climate change on surface runoff response using gridded observations and SWAT+. Hydrology 8, 48. https://doi.org/10.3390/hydrology8010048.
Kishawi, Y., Mittelstet, A.R., Gilmore, T.E., Twidwell, D., Roy, T., Shrestha, N., 2023. Impact of eastern redcedar encroachment on water resources in the Nebraska sandhills. Sci. Total Environ. 858, 159696 https://doi.org/10.1016/j.scitotenv.2022.159696.
Knapp, A.K., Conard, S.L., Blair, J.M., 1998. Determinants of soil Co2 flux from a sub-humid grassland: effect of fire and fire history. Ecol. Appl. 8, 760–770. https://doi.org/10.1890/1051-0761(1998)008[0760:DOSCFF]2.0.CO;2.
Lee, S., Ajami, H., 2023. Comprehensive assessment of baseflow responses to long-term meteorological droughts across the United States. J. Hydrol. 626, 130256 https://doi.org/10.1016/j.jhydrol.2023.130256.
Liu, H., Xu, C., Allen, C.D., Hartmann, H., Wei, X., Yakir, D., Wu, X., Yu, P., 2022. Nature-based framework for sustainable afforestation in global drylands under changing climate. Global Change Biol. 28, 2202–2220. https://doi.org/10.1111/gcb.16059.
Livneh, B., Hoerling, M.P., 2016. The physics of drought in the U.S. Central Great Plains. J. Clim. 29, 6783–6804. https://doi.org/10.1175/JCLI-D-15-0697.1.
Middleton, N., Thomas, D., 1997. World Atlas of Desertification. Arnold, Hodder Headline, PLC, 2.
Moriasi, D.N., Arnold, J.G., Van Liew, M.W., Bingner, R.L., Harmel, R.D., Veith, T.L., 2007. Model evaluation guidelines for systematic quantification of accuracy in watershed simulations. Transactions of the ASABE 50, 885–900.
Morton, L.W., Regen, E., Engle, D.M., Miller, J.R., Harr, R.N., 2010. Perceptions of landowners concerning conservation, grazing, fire, and eastern redcedar management in tallgrass prairie. Rangel. Ecol. Manag. 63, 645–654. https://doi.org/10.2111/REM-D-09-00041.1.
Nave, L.E., Domke, G.M., Hofmeister, K.L., Mishra, U., Perry, C.H., Walters, B.F., Swanston, C.W., 2018. Reforestation can sequester two petagrams of carbon in US topsoils in a century. Proc. Natl. Acad. Sci. USA 115, 2776–2781. https://doi.org/10.1073/pnas.1719685115.
Ouyang, Y., Jin, W., Leininger, T.D., Feng, G., Yang, J., 2021. Impacts of afforestation on groundwater resource: a case study for Upper Yazoo River watershed, Mississippi, USA. Hydrol. Sci. J. 66, 464–473. https://doi.org/10.1080/02626667.2021.1876235.
Pan, S., Yang, J., Tian, H., Shi, H., Chang, J., Ciais, P., Francois, L., Frieler, K., Fu, B., Hickler, T., Ito, A., Nishina, K., Ostberg, S., Reyer, C.P.O., Schaphoff, S., Steinkamp, J., Zhao, F., 2020. Climate extreme versus carbon extreme: responses of terrestrial carbon fluxes to temperature and precipitation. J. Geophys. Res.: Biogeosciences 125, e2019JG005252. https://doi.org/10.1029/2019JG005252.
Pan, Y., Birdsey, R.A., Fang, J., Houghton, R., Kauppi, P.E., Kurz, W.A., Phillips, O.L., Shvidenko, A., Lewis, S.L., Canadell, J.G., Ciais, P., Jackson, R.B., Pacala, S.W., McGuire, A.D., Piao, S., Rautiainen, A., Sitch, S., Hayes, D., 2011. A large and persistent carbon sink in the world's forests. Science 333, 988–993. https://doi.org/10.1126/science.1201609.
Payton, E.A., Pinson, A.O., Asefa, T., Condon, L.E., Dupigny-Giroux, L., Harding, B., Kiang, J., Lee, D.H., McAfee, S.A., Pflug, J.M., Rangwala, I., Tanana, H., Wright, D., 2023. Ch. 4. Water. In: Fifth National Climate Assessment. U.S. Global Change Research Program. Washinton, DC.
Phillips, S.J., Dudík, M., 2008. Modeling of species distributions with Maxent: new extensions and a comprehensive evaluation. Ecography 31, 161–175. https://doi.org/10.1111/j.0906-7590.2008.5203.x.
Piao, S., Friedlingstein, P., Ciais, P., de Noblet-Ducoudré, N., Labat, D., Zaehle, S., 2007. Changes in climate and land use have a larger direct impact than rising CO2 on global river runoff trends. Proc. Natl. Acad. Sci. USA 104, 15242–15247. https://doi.org/10.1073/pnas.0707213104.

Prudhomme, C., Davies, H., 2009. Assessing uncertainties in climate change impact analyses on the river flow regimes in the UK. Part 2: future climate. Climatic Change 93, 197–222. https://doi.org/10.1007/s10584-008-9461-6.
Pulighe, G., Lupia, F., Chen, H., Yin, H., 2021. Modeling climate change impacts on water balance of a mediterranean watershed using SWAT+. Hydrology 8, 157. https://doi.org/10.3390/hydrology8040157.
Qiao, L., Zou, C.B., Stebler, E., Will, R.E., 2017. Woody plant encroachment reduces annual runoff and shifts runoff mechanisms in the tallgrass prairie, USA. Water Resour. Res. 53, 4838–4849. https://doi.org/10.1002/2016WR019951.
Qiao, L., Zou, C.B., Will, R.E., Stebler, E., 2015. Calibration of SWAT model for woody plant encroachment using paired experimental watershed data. J. Hydrol. 523, 231–239. https://doi.org/10.1016/j.jhydrol.2015.01.056.
Robertson, G.P., Hamilton, S.K., Paustian, K., Smith, P., 2022. Land-based climate solutions for the United States. Global Change Biol. 28, 4912–4919. https://doi.org/10.1111/gcb.16267.
Rodríguez, E., Morris, C.S., Belz, J.E., 2006. A global assessment of the SRTM performance. Photogramm. Eng. Rem. Sens. 72, 249–260. https://doi.org/10.14358/PERS.72.3.249.
Sankaran, M., Hanan, N.P., Scholes, R.J., Ratnam, J., Augustine, D.J., Cade, B.S., Gignoux, J., Higgins, S.I., Le Roux, X., Ludwig, F., Ardo, J., Banyikwa, F., Bronn, A., Bucini, G., Caylor, K.K., Coughenour, M.B., Diouf, A., Ekaya, W., Feral, C.J., February, E.C., Frost, P.G.H., Hiernaux, P., Hrabar, H., Metzger, K.L., Prins, H.H.T., Ringrose, S., Sea, W., Tews, J., Worden, J., Zambatis, N., 2005. Determinants of woody cover in African savannas. Nature 438, 846–849. https://doi.org/10.1038/nature04070.
Scholtz, R., Fuhlendorf, S.D., Uden, D.R., Allred, B.W., Jones, M.O., Naugle, D.E., Twidwell, D., 2021. Challenges of brush management treatment effectiveness in southern Great Plains, United States. Rangel. Ecol. Manag. 77, 57–65. https://doi.org/10.1016/j.rama.2021.03.007.
Schubert, S.D., Suarez, M.J., Pegion, P.J., Koster, R.D., Bacmeister, J.T., 2004. On the cause of the 1930s dust Bowl. Science 303, 1855–1859. https://doi.org/10.1126/science.1095048.
Sheil, D., 2018. Forests, atmospheric water and an uncertain future: the new biology of the global water cycle. For. Ecosyst. 5, 19. https://doi.org/10.1186/s40663-018-0138-y.
Shi, X., Mao, J., Thornton, P.E., Hoffman, F.M., Post, W.M., 2011. The impact of climate, CO2, nitrogen deposition and land use change on simulated contemporary global river flow. Geophys. Res. Lett. 38 https://doi.org/10.1029/2011GL046773.
Silver, W.L., Ostertag, R., Lugo, A.E., 2000. The potential for carbon sequestration through reforestation of abandoned tropical agricultural and pasture lands. Restor. Ecol. 8, 394–407. https://doi.org/10.1046/j.1526-100x.2000.80054.x.
Starr, M., Joshi, O., Will, R.E., Zou, C.B., 2019. Perceptions regarding active management of the Cross-timbers forest resources of Oklahoma, Texas, and Kansas: a SWOT-ANP analysis. Land Use Pol. 81, 523–530. https://doi.org/10.1016/j.landusepol.2018.11.004.
Tabari, H., 2020. Climate change impact on flood and extreme precipitation increases with water availability. Sci. Rep. 10, 13768 https://doi.org/10.1038/s41598-020-70816-2.
Taylor, K.E., Stouffer, R.J., Meehl, G.A., 2012. An overview of CMIP5 and the experiment design. Bull. Am. Meteorol. Soc. 93, 485–498. https://doi.org/10.1175/BAMS-D-11-00094.1.
Tolson, B.A., Shoemaker, C.A., 2007. Dynamically dimensioned search algorithm for computationally efficient watershed model calibration. Water Resour. Res. 43 https://doi.org/10.1029/2005WR004723.
Trabucco, A., Zomer, R.J., Bossio, D.A., van Straaten, O., Verchot, L.V., 2008. Climate change mitigation through afforestation/reforestation: a global analysis of hydrologic impacts with four case studies. Agriculture, Ecosystems & Environment, International Agricultural Research and Climate Change: A Focus on Tropical Systems 126, 81–97. https://doi.org/10.1016/j.agee.2008.01.015.
Twidwell, D., Fuhlendorf, S.D., Taylor Jr, C.A., Rogers, W.E., 2013. Refining thresholds in coupled fire–vegetation models to improve management of encroaching woody plants in grasslands. J. Appl. Ecol. 50, 603–613. https://doi.org/10.1111/1365-2664.12063.
van Vliet, M.T.H., Franssen, W.H.P., Yearsley, J.R., Ludwig, F., Haddeland, I., Lettenmaier, D.P., Kabat, P., 2013. Global river discharge and water temperature under climate change. Global Environ. Change 23, 450–464. https://doi.org/10.1016/j.gloenvcha.2012.11.002.
Wang, J., Xiao, X., Qin, Y., Dong, J., Geissler, G., Zhang, G., Cejda, N., Alikhani, B., Doughty, R.B., 2017. Mapping the dynamics of eastern redcedar encroachment into grasslands during 1984–2010 through PALSAR and time series Landsat images. Rem. Sens. Environ. 190, 233–246. https://doi.org/10.1016/j.rse.2016.12.025.
Wang, J., Xiao, X., Qin, Y., Doughty, R.B., Dong, J., Zou, Z., 2018a. Characterizing the encroachment of juniper forests into sub-humid and semi-arid prairies from 1984 to 2010 using PALSAR and Landsat data. Rem. Sens. Environ. 205, 166–179. https://doi.org/10.1016/j.rse.2017.11.019.
Wang, J., Xiao, X., Zhang, Y., Qin, Y., Doughty, R.B., Wu, X., Bajgain, R., Du, L., 2018b. Enhanced gross primary production and evapotranspiration in juniper-encroached grasslands. Global Change Biol. 24, 5655–5667. https://doi.org/10.1111/gcb.14441.
Wang, Q., Cheng, L., Zhang, L., Liu, P., Qin, S., Liu, L., Jing, Z., 2021. Quantifying the impacts of land-cover changes on global evapotranspiration based on the continuous remote sensing observations during 1982–2016. J. Hydrol. 598, 126231 https://doi.org/10.1016/j.jhydrol.2021.126231.
Wilcox, B.P., 2002. Shrub control and streamflow on rangelands: a process based viewpoint. J. Range Manag. 55.
Wilcox, B.P., Birt, A., Archer, S.R., Fuhlendorf, S.D., Kreuter, U.P., Sorice, M.G., van Leeuwen, W.J.D., Zou, C.B., 2018. Viewing woody-plant encroachment through a social–ecological lens. Bioscience 68, 691–705. https://doi.org/10.1093/biosci/biy051.
Wu, Y., Liu, S., Abdul-Aziz, O.I., 2012. Hydrological effects of the increased CO2 and climate change in the Upper Mississippi River Basin using a modified SWAT. Climatic Change 110, 977–1003. https://doi.org/10.1007/s10584-011-0087-8.
Xu, H., Yue, C., Zhang, Y., Liu, D., Piao, S., 2023. Forestation at the right time with the right species can generate persistent carbon benefits in China. Proc. Natl. Acad. Sci. USA 120, e2304988120. https://doi.org/10.1073/pnas.2304988120.
Yang, J., Will, R., Zou, C., Zhai, L., Winrich, A., Fang, S., 2024. Eastward shift in Juniperus virginiana distribution range under future climate conditions in the Southern Great Plains, United States. Agric. For. Meteorol. 345, 109836 https://doi.org/10.1016/j.agrformet.2023.109836.
Yang, J., Zou, C., Will, R., Wagner, K., Ouyang, Y., King, C., Winrich, A., Tian, H., 2023. River flow decline across the entire Arkansas River Basin in the 21st century. J. Hydrol. 618, 129253 https://doi.org/10.1016/j.jhydrol.2023.129253.
Zhang, R., Fujimori, S., 2020. The role of transport electrification in global climate change mitigation scenarios. Environ. Res. Lett. 15, 034019 https://doi.org/10.1088/1748-9326/ab6658.
Zhang, Y., Qi, J., Pan, D., Marek, G.W., Zhang, X., Feng, P., Liu, H., Li, B., Ding, B., Brauer, D.K., Srinivasan, R., Chen, Y., 2022. Development and testing of a dynamic CO2 input method in SWAT for simulating long-term climate change impacts across various climatic locations. J. Hydrol. 614, 128544 https://doi.org/10.1016/j.jhydrol.2022.128544.
Zou, C.B., Qiao, L., Wilcox, B.P., 2016. Woodland expansion in central Oklahoma will significantly reduce streamflows – a modelling analysis. Ecohydrology 9, 807–816. https://doi.org/10.1002/eco.1684.
Zou, C.B., Turton, D.J., Will, R.E., Engle, D.M., Fuhlendorf, S.D., 2014. Alteration of hydrological processes and streamflow with juniper (Juniperus virginiana) encroachment in a mesic grassland catchment. Hydrol. Process. 28, 6173–6182. https://doi.org/10.1002/hyp.10102.